Surface Science 167 (1986) 341–362
North-Holland, Amsterdam

EFFECTS OF LASER PULSE CHARACTERISTICS AND THERMAL DESORPTION PARAMETERS ON LASER INDUCED THERMAL DESORPTION

J.L. BRAND and S.M. GEORGE
Department of Chemistry, Stanford University, Stanford, California 94305, USA

Received 18 June 1985; accepted for publication 5 November 1985

The effects of laser pulse characteristics and thermal desorption parameters on laser induced thermal desorption (LITD) are determined. The LITD is calculated for model first and second order desorption systems with laser pulses that are Gaussian in space and time. The desorption yields and coverage profiles generated by LITD are shown to be sensitively dependent on laser pulse characteristics and thermal desorption kinetics. The calculations also reveal that the desorption flux generated by LITD possesses a distribution of desorption temperatures. In addition, the relationships between the laser pulselength, the peak temperature reached on the surface, and the desorption activation energy are determined.

1. Introduction

Laser induced thermal desorption (LITD) is a technique that has displayed widespread utility in the preparation of surfaces and in the study of processes on surfaces. Studies have shown the feasibility of using LITD to clean and anneal surfaces [1–5], to analyze adsorbates on surfaces [6–8], and to desorb and ionize large organic molecules when conventional ionization methods promote decomposition [9–14]. LITD has also proved useful in the study of surface desorption and adsorption kinetics [15–25], surface diffusion [26,27], and as a real-time probe of surface reaction kinetics [28].

In order to initiate LITD, a surface is irradiated with a laser pulse. Depending on the optical properties of the surface, a portion of the laser pulse energy is transmitted into the surface. The absorbed light energy heats the surface and produces a temperature jump. If the induced temperature jump has a sufficient magnitude and duration, adsorbates can be thermally desorbed from the surface.

Laser heating is able to heat surfaces at rates unattainable with traditional surface heating methods. Using conventional resistive or electron bombardment heating, heating rates of only $1–10^3$ K/s can be attained. LITD allows the surface to be heated at rates up to 10^{11} K/s with nanosecond laser pulses

0039-6028/86/$03.50

and even faster with picosecond laser pulses. For adsorbates that undergo decomposition at a conventional heating rate of 10 K/s, the rapid laser induced heating rates can favor desorption over decomposition. This has enabled the time dependence of chemical reactions to be analyzed [28] and the mass analysis of large organic compounds to be studied [9–14].

Because laser pulses can be focused onto a small area of a surface, laser heating permits significant temperature gradients to be created. The subsequent LITD occurs only from the irradiated area of the surface and a coverage gradient is produced on the surface. These coverage gradients enable a wide range of experiments to be performed that are not possible using conventional heating. Recently, coverage gradients produced by LITD have been used to study surface diffusion [26,27].

Despite the usefulness of LITD, the effects of laser pulse characteristics and thermal desorption parameters on LITD have not been examined sufficiently. In particular, the effect of these characteristics and parameters on the spatial profile of the surface coverage remaining after LITD has not been explored. In response to this situation, the desorption yields and resultant coverage profiles remaining after LITD have been calculated, and the dependence on the laser pulse characteristics and thermal desorption kinetics has been demonstrated.

2. Calculations

2.1. Laser pulse characteristics

The surface coverage profile established by LITD is intimately related to the spatial and temporal characteristics of the laser pulse. In these calculations we have employed a laser pulse intensity that is Gaussian both in space and in time:

$$I(r,\ t) = I_0\, \mathrm{e}^{-4(\ln 2)(r/r_\mathrm{p})^2}\ \mathrm{e}^{-4(\ln 2)(t/t_\mathrm{p})^2}. \tag{1}$$

In this expression, I_0 is the peak laser intensity at the center of the spatial distribution, t_p is the FWHM temporal pulselength and r_p is the FWHM spatial pulsewidth. A Gaussian temporal distribution is a close approximation to laser pulses from most pulsed lasers [29,30]. A Gaussian spatial distribution is a close approximation to laser pulses from laser resonators limited to the TEM_{00} transverse mode [31].

The calculations emphasize Gaussian spatial distributions, and comparisons to uniform spatial distributions are given. Although uniform spatial distributions are easier to model and are preferred experimentally, they cannot be obtained by transmitting a fraction of an expanded laser beam through an aperture. Light always penetrates the geometrical shadow region due to diffraction effects and gives rise to a non-uniform spatial distribution both in the near

field [32] and the far field [33]. The spatial extent of these diffraction effects is given approximately by $x\lambda/D$, where λ is the wavelength and x is the distance from an aperture of diameter D [32,33]. As the apertured beam propagates to the far field or to a focal point of a lens, the spatial intensity distribution will become approximately Gaussian [33–35].

The total energy of the laser pulse may be calculated by integrating the intensity over the entire area and over all time. This gives the total energy of the laser pulse as:

$$E = \left[\sqrt{\pi^3}/8\sqrt{(\ln 2)^3}\right] I_0 t_p r_p^2. \tag{2}$$

Experimentally, measuring the total energy of the laser pulse is easier than measuring the intensity; hence, eq. (2) may be rearranged to solve for the peak laser intensity given the laser pulse energy, pulselength, and pulsewidth.

Many comparisons between different laser pulselengths are given in this study. However, these calculations emphasize laser pulselengths with $t_p = 100$ ns. These pulselengths are longer than the pulselengths commonly produced by Q-switched lasers. As will be shown, there are significant advantages to using longer pulselengths in order to lower peak surface temperatures and reduce the likelihood of laser-induced surface damage. These longer pulselengths can be attained by modifying conventional Q-switched lasers [36].

2.2. Laser induced surface heating

The equations to describe laser induced surface heating have been derived previously [37,38]. For this study, the temperature was calculated only at the surface using an equation that was derived for a heat source at the surface of a semi-infinite solid [37]:

$$T(t) = \frac{1-R}{\sqrt{(K\rho c\pi)}} \int_0^t \frac{I(t-t')}{\sqrt{t'}}\,\mathrm{d}t' + T_0. \tag{3}$$

In this equation R is the reflectivity, K is the thermal conductivity, c is the heat capacity, ρ is the density, and $I(t-t')$ is the temporal distribution of the incident laser intensity. Ruthenium is a typical Group VIII metal and was used as the model surface for representative optical and thermal properties. For ruthenium at $\lambda = 1.06$ μm, the thermal properties are $K = 1.17$ W/cm · K, $c = 0.238$ J/g · K, $\rho = 12.2$ g/cm^3, [39] and the reflectivity is $(1-R) = 0.38$ [40]. The assumptions limiting this equation have been discussed previously [10,17,18,20,28,37,41].

Fig. 1a shows the calculated laser induced temperature excursion for a 100 nanosecond laser pulse with an incident peak intensity I_0 of 23.5 MW/cm^2 and an initial surface temperature of 250 K. The temporal Gaussian laser pulse intensity is superimposed on the temperature excursion. Fig. 1b shows the

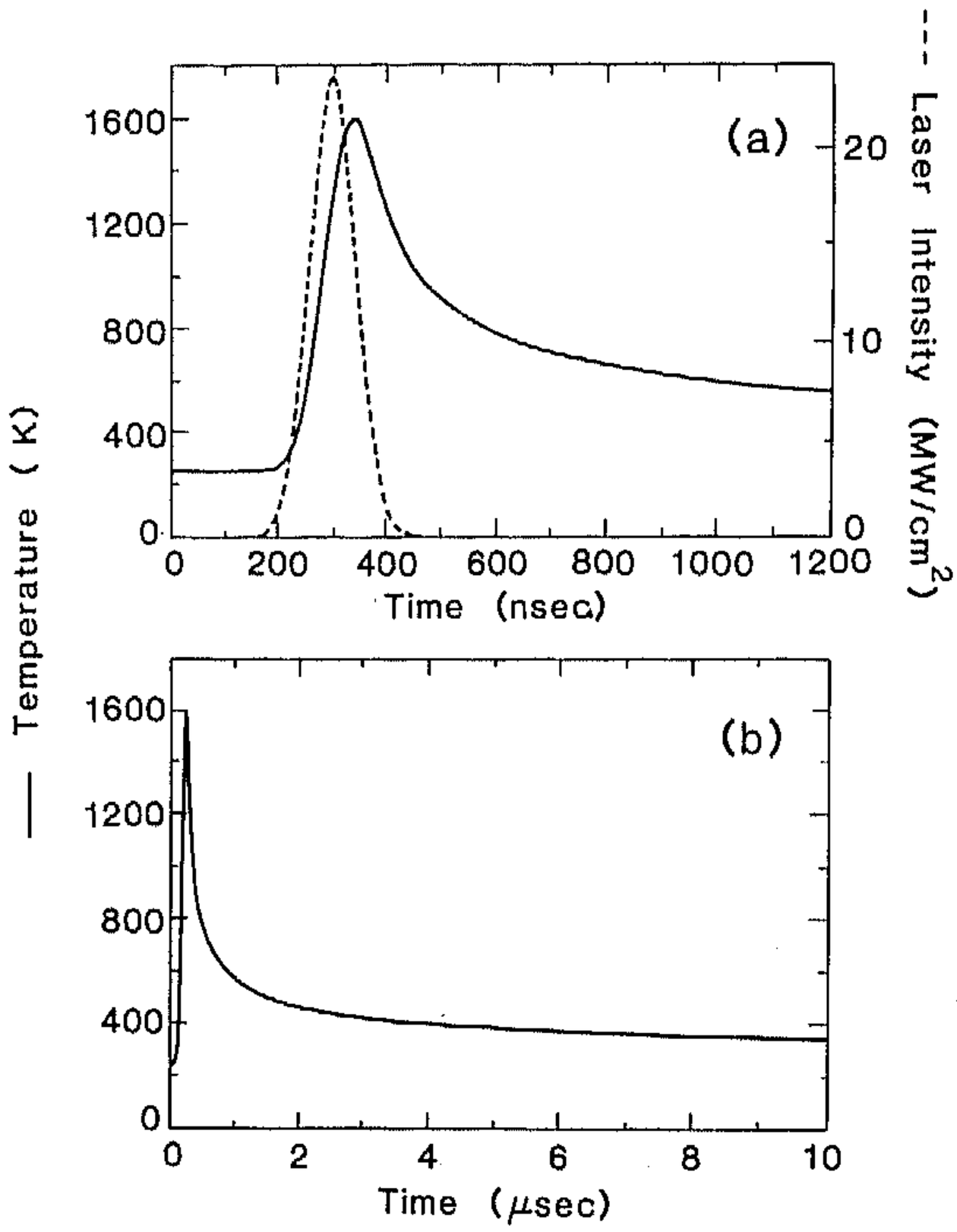

Fig. 1. (a) The temperature excursion calculated for a 100 ns laser pulse with a peak intensity of 23.5 MW/cm^2 on a ruthenium surface with an initial temperature of 250 K. The Gaussian temporal profile of the laser pulse is superimposed on the temperature excursion. (b) The same temperature excursion over a longer time scale.

same laser induced temperature excursion over a much longer time scale. This calculation demonstrates that the surface temperature returns to the initial surface temperature in 50 to 100 pulselengths.

For longer times, the equation calculates temperatures that are higher than those that would be measured. This overestimation occurs because heat was not allowed to diffuse laterally in the evaluation of eq. (3). The root-mean square distance for lateral heat diffusion is $X = 2\sqrt{(\kappa t)}$ [42]. For a typical Group VIII metal with $\kappa = 0.4$ cm^2/s, heat will diffuse $\simeq 40$ μm in 10 μs. Thus, lateral heat diffusion may reduce substantially the temperature predicted by eq. (3) for longer times or for tightly-focused laser pulses, e.g. a 1 μs laser pulse focused to $\simeq 50$ μm diameter or a 10 ns pulse focused to $\simeq 5$ μm diameter.

There are two empirical results from these calculations for laser heating. First, the peak temperature occurs about 35% of the pulselength after the maximum laser intensity:

$$t(T_{\text{peak}}) \simeq 0.35 t_{\text{p}}. \tag{4}$$

Bechtel reported that the T_{peak} occurs at $\approx 0.55t_p$, but this resulted from his different definition of the pulselength [41]. Other calculations for Gaussian laser pulses reported a peak temperature at $0.325t_p$ [18].

Second, the peak temperature for any Gaussian laser pulse may be calculated by the following relationship:

$$T_{peak} = 49.5 \frac{1 - R}{\sqrt{(K\rho c\pi)}} I_0 \sqrt{t_p} + T_0, \tag{5}$$

where I_0 is in MW/cm^2 and t_p is in nanoseconds. For the model ruthenium surface with light energy at $\lambda = 1.06\ \mu$m, this relationship becomes:

$$T_{peak} = 5.76 I_0 \sqrt{t_p} + T_0, \tag{6}$$

where I_0 is in MW/cm^2, t_p is in nanoseconds and the constant has units of cm^{2}K/MW $\cdot$ s$^{1/2}$.

2.3. Laser induced thermal desorption

The rate equation for thermal desorption is:

$$-\mathrm{d}\Theta/\mathrm{d}t = \nu_n \Theta^n \, \mathrm{e}^{-E_d/RT}, \tag{7}$$

where Θ is the surface concentration, n is the order of the desorption, ν is the pre-exponential, and E_d is the desorption activation energy [43]. Typically, the thermal desorption rate equations are rewritten in terms of a constant heating rate $\beta = \mathrm{d}T/\mathrm{d}t$. However, for LITD, β is impossible to define because the laser induced heating rate is not constant in time. Moreover, given a Gaussian spatial distribution for the laser beam, the heating rate also varies at different positions on the surface. Consequently, eq. (3) was utilized to determine the temperature excursion at different spatial positions. After the temperature excursions were determined, eq. (7) was used to calculate the thermal desorption.

3. Spatial profile results

3.1. Model systems

Thermal desorption usually exhibits either first or second order kinetics. The values of the thermal desorption parameters for the first order model system are representative of first order desorption systems such as CO and NO with desorption activation energies of 30 kcal/mol and pre-exponentials of 10^{13}/s [44–46]. Likewise, for the second order model system, thermal desorption values are representative of second order recombinatory desorption sys-

Table 1
Model parameters for LITD

	First order	Second order
Desorption activation energy (kcal/mol)	30	15
Pre-exponential (s^{-1})	10^{13}	10^{-3} cm^2/adsorbate
Initial coverage (adsorbates/cm^2)	3.18×10^{14}	3.18×10^{14}
Initial temperature (K)	250	250
Temporal pulselength (ns)	100	100
Spatial pulsewidth (μm)	400	400
Peak laser intensity (MW/cm^2)	23.5	13.8

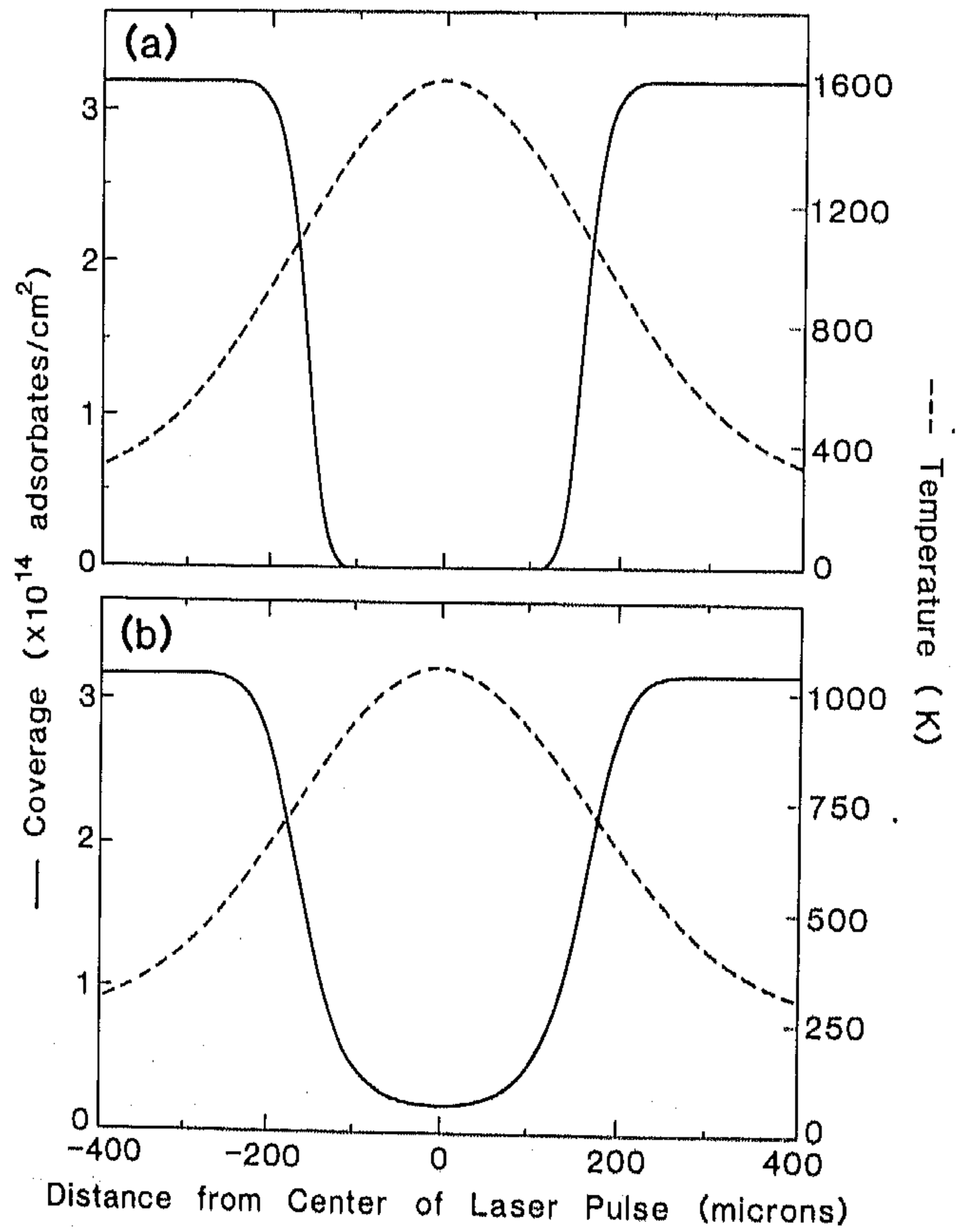

Fig. 2. The spatial profile of the resultant adsorbate coverage on the surface following LITD and the peak temperature reached at each spatial position for the two model systems: (a) first order; (b) second order.

tems such as hydrogen and methanol with desorption activation energies of 15 kcal/mol and pre-exponentials of 10^{-3} cm^2/adsorbate · s [45–48]. The model desorption parameters are given in table 1. The initial coverage corresponds to approximately 20% of a monolayer on a Ru(001) surface. Laser induced temperature excursions were calculated for the model ruthenium surface. Because the thermal and optical properties of the Group VIII metals are similar, these calculated temperature excursions are typical for these metals.

Fig. 2 shows the spatial coverage profiles established by laser induced thermal, desorption for the two model systems. The peak laser intensities for (a) and (b) were chosen in order that one-half of the initial adsorbates were desorbed at the spatial position $r = 0.4r_p$. The position where the adsorbates are "half-desorbed" provides a simple criterion to describe the radius of the coverage profile when the coverage is completely or almost completely desorbed at the center of the profile.

A comparison of figs. 2a and 2b shows that the first order desorption system burns out a much deeper area. Furthermore, the transition from near zero coverage to the initial coverage occurs over a shorter distance for the first order system. This is a direct result of the thermal desorption kinetics. Second order desorption requires two adsorbed species to diffuse together and desorb recombinatively. As the coverage is depleted, the mean square distance between any two adsorbed species is increased and the probability of desorption is decreased.

3.2. *The dynamics of LITD*

Conventional temperature programmed desorption utilizes a constant, slow heating rate. The desorption temperatures are given by the time at which the adsorbate is detected. This is not the case with LITD. Because the heating rates and the peak temperatures vary across the spatial intensity distribution, desorption occurs at different times and temperatures for each spatial position.

Fig. 3a shows the temporal profile of the desorption flux from different spatial positions for the first order model system. Each desorption flux peak is weighted according to its distance from the center of the laser beam. Notice that, due to the Gaussian spatial distribution of the laser beam on the surface, the adsorbates at the center of the pulse are desorbed first and those at the edge are desorbed last.

The calculations also show that the adsorbates are desorbed from the surface over a wide range of temperatures. This distribution of temperatures results both from the various temperature excursions occurring at different spatial positions and from the range of desorption temperatures occurring at each spatial position. The total temperature distribution and the temperature distribution from different spatial positions for the first order model system are shown in fig. 3b.

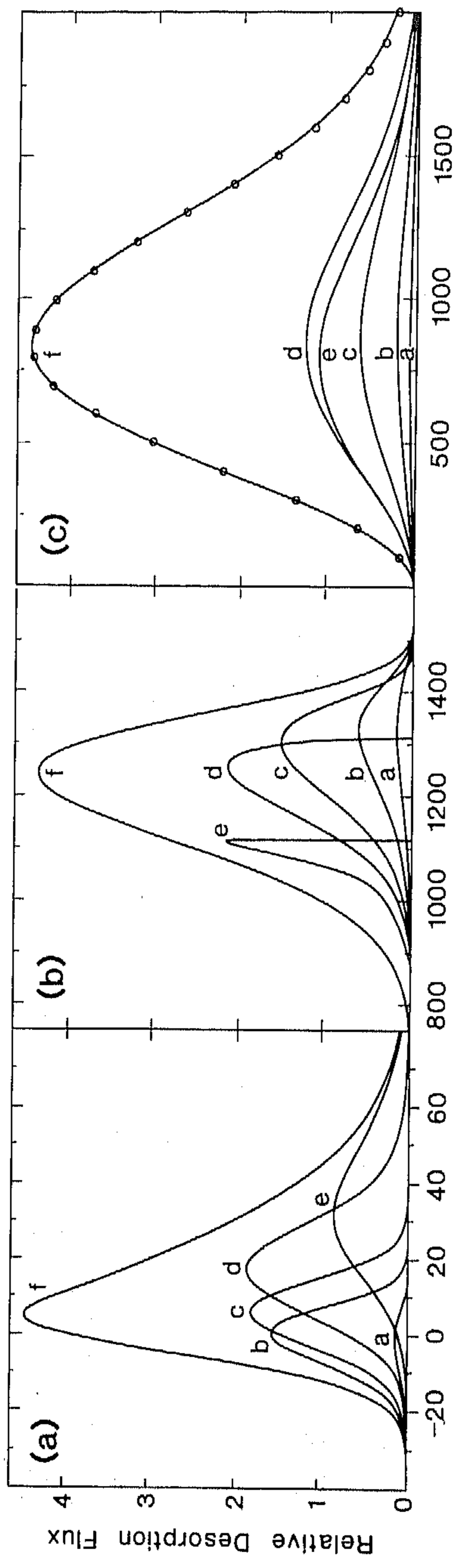

Fig. 3. (a) The desorption flux of adsorbates leaving the surface as a function of time at different spatial positions. The peaks correspond to: (a) $r = 0$; (b) $r = 0.1r_p$; (c) $r = 0.2r_p$; (d) $r = 0.3r_p$; (e) $r = 0.4r_p$. The peak labeled f represents the total desorption flux from the surface. (b) The distribution of desorption temperatures comprising the desorption flux. (c) The velocity distribution of the adsorbates leaving the surface. The open circles correspond to a Maxwell–Boltzmann distribution at $T = 1190$ K.

The peak desorption flux at the center of the laser pulse occurs significantly below the peak surface temperature. Fig. 3b illustrates that the desorption flux at the center of the laser pulse is distributed over a wide range of temperatures and is peaked at 1350 K while the peak surface temperature occurs at $T_p = 1600$ K. On the other hand, at the edge of the spatial profile ($r = 0.4r_p$) the desorption flux is distributed over a narrower range of temperatures at and below 1120 K, which is also the peak temperature at that point.

The distribution of desorption temperatures comprising the total desorption flux, f in fig. 3b, is a slightly skewed distribution with a peak at 1250 K. The desorbed particles leave the surface with a wide range of temperatures and, therefore, a wide distribution of thermal velocities. Each temperature gives rise to a Maxwell–Boltzmann velocity distribution [49,50] according to:

$$dF(v, t) = N(T)\, 4\pi (m/2\pi kT)^{3/2} v^2\, e^{-mv^2/2kT}\, dv\, dT. \tag{8}$$

The variables represent the standard meanings with $N(T)$ being the desorption flux at temperature T. Transforming each temperature into a weighted Maxwell–Boltzmann velocity distribution and integrating over the entire temperature distribution yields the total velocity distribution for the desorbed flux shown in fig. 3c. A mass of 28 AMU (CO or N_2) was assumed.

A comparison between the velocity distribution for the total desorption flux shown in fig. 3c and a Maxwell–Boltzmann velocity distribution for particles at only $T = 1190$ K reveals that the distributions are nearly identical. This occurs even though the velocity distribution for the desorption flux arose from a distribution of temperatures with a peak at 1250 K and not one temperature. Therefore, the measured velocity distribution in time-of-flight LITD experiments can not be assigned unambiguously to one characteristic temperature even though attempts to fit measured velocity distributions to one temperature have been made [17,20,21,28,51,52].

A uniform spatial distribution yields less complicated results than those for a Gaussian spatial distribution. For example, a uniform laser intensity of 18.3 MW/cm^2 with a 100 ns Gaussian FWHM temporal pulselength is sufficient to desorb nearly all the adsorbates characterized by the first order model system. The desorption dynamics for a uniform spatial distribution of 18.3 MW/cm^2 are equivalent to those shown by line d in fig. 3. This equivalence occurs because line d corresponds to a peak intensity of 18.3 MW/cm^2 on the Gaussian spatial distribution.

Fig. 4 shows the same series of calculations as in fig. 3. In this case, a 10 ns laser pulse with a higher peak intensity was used to create the same size coverage profile ($r = 0.4r_p$). The shorter temporal pulselength creating the same coverage profile results in an even greater temperature range for desorption. The resultant total velocity distribution again appears to be a Maxwell–Boltzmann distribution from one temperature. For the 10 ns laser

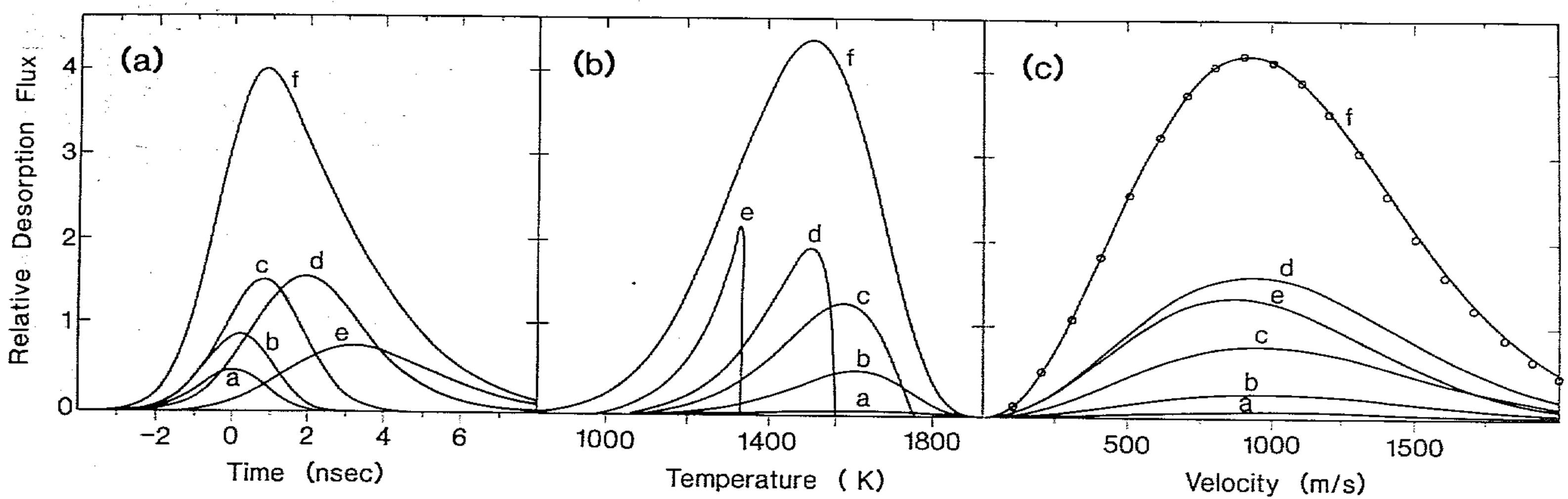

Fig. 4. Calculations for a 10 ns laser pulse with a peak intensity of 92.3 MW/cm^2 and a peak surface temperature of 1930 K. (a) The desorption flux of adsorbates leaving the surface as a function of time at different spatial positions. The peaks correspond to: (a) $r = 0$; (b) $r = 0.1r_p$; (c) $r = 0.2r_p$; (d) $r = 0.3r_p$; (e) $r = 0.4r_p$. The peak labeled f represents the total desorption flux from the surface. (b) The distribution of desorption temperature comprising the total desorption flux. (c) The velocity distribution of the adsorbates leaving the surface. The open circles correspond to a Maxwell–Boltzmann distribution at 1400 K.

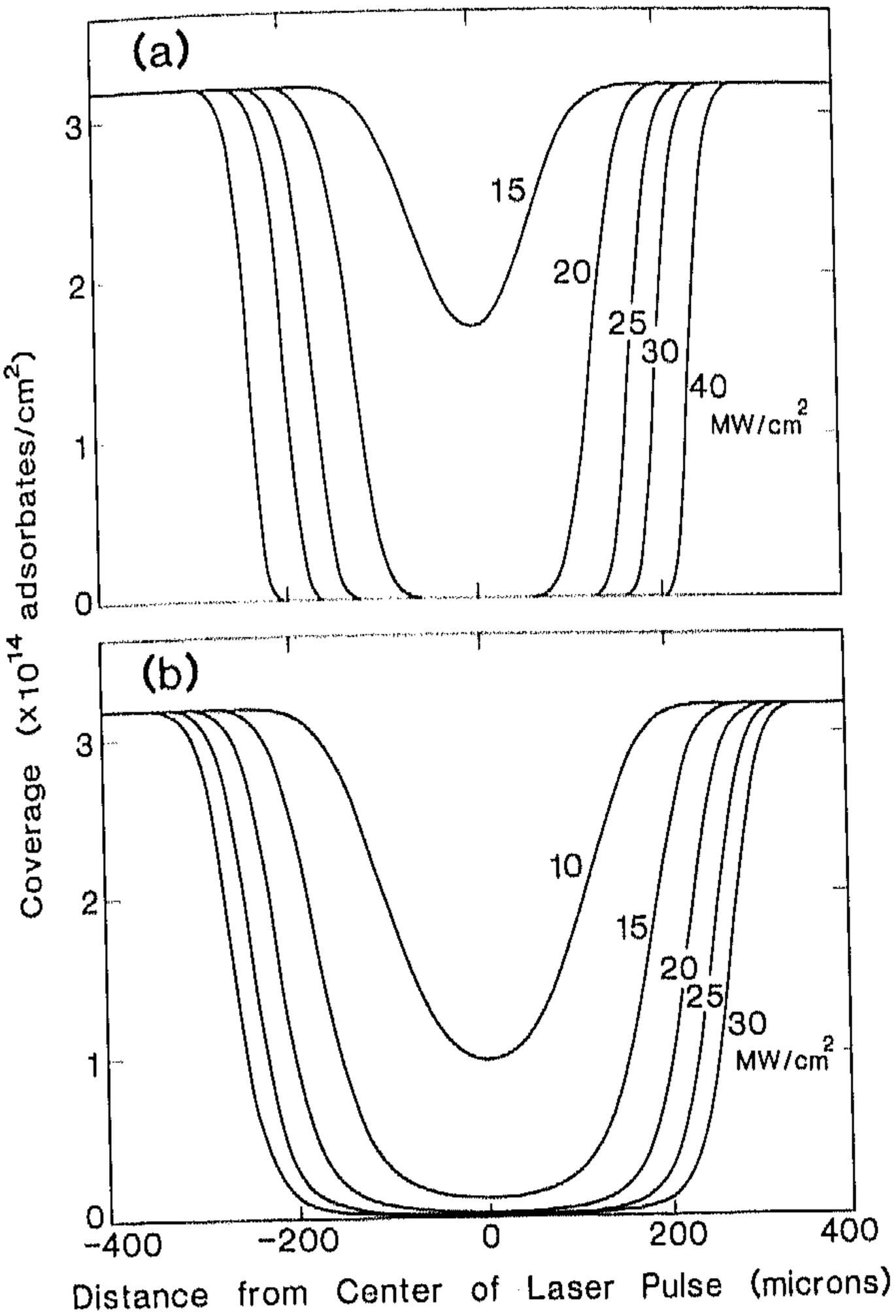

Fig. 5. The effect of changing the peak incident laser intensity on the resultant coverage profile. (a) First order model system; (b) second order model system.

pulse, the peak surface temperature is 1900 K, the velocity distribution fits a Maxwell–Boltzmann temperature of 1400 K, and the molecules desorb over a wide distribution of temperatures ranging from 1100–1800 K.

3.3. *Effects of laser pulse characteristics*

Given a particular adsorbate–substrate system, an experimenter can only change the laser intensity, the pulselength, and the initial surface temperature. Fig. 5 shows how changes in the peak incident laser intensity affect the coverage profile. A threshold intensity must be reached before any thermal desorption can occur. As the laser intensity is increased the coverage profile becomes wider and the edges of the coverage profile become steeper. The edges are always steeper for the first order system than for the second order model

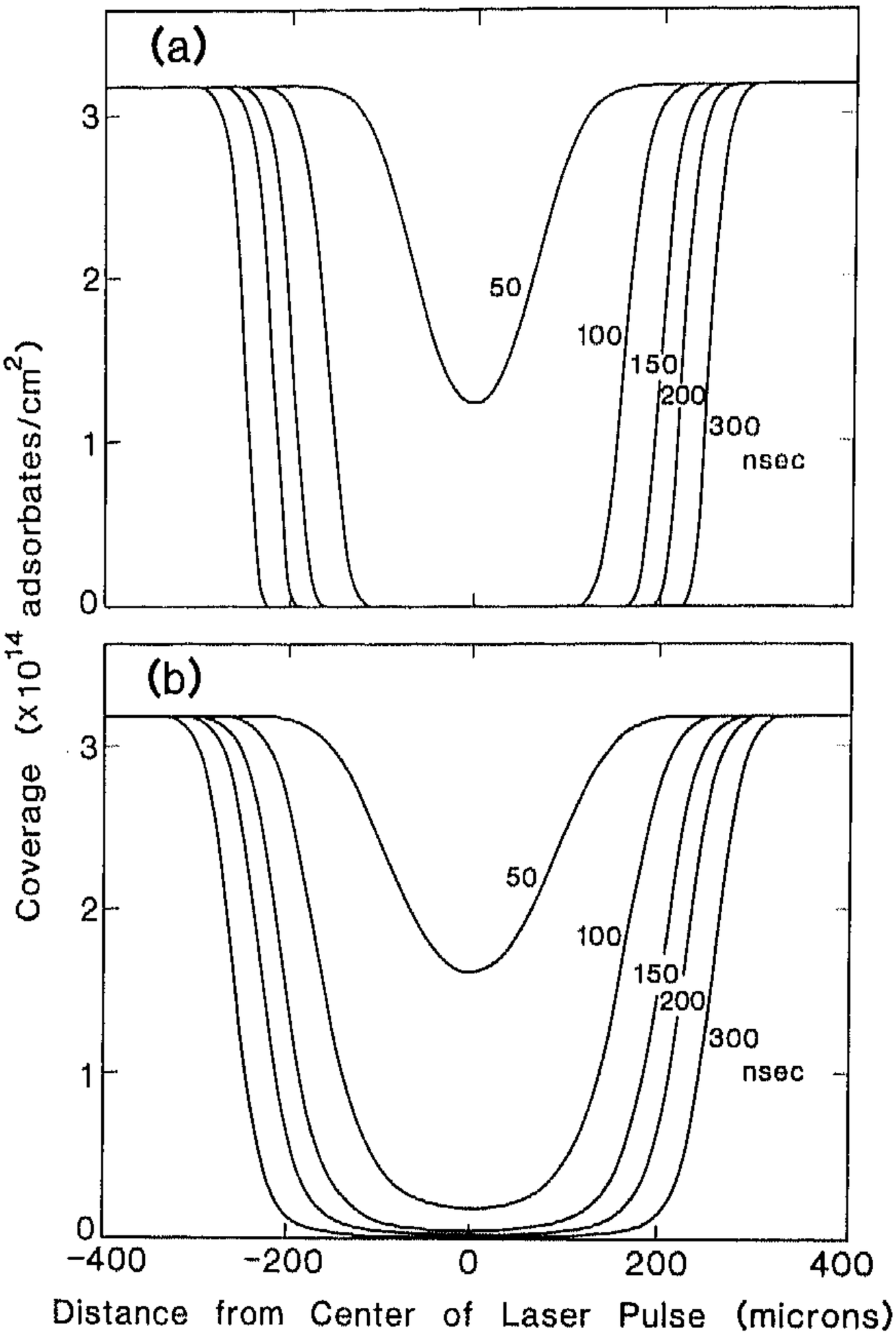

Fig. 6. The effect of changing the pulselength on the resultant coverage profile. Each pulse has a peak incident laser intensity of (a) 23.5 MW/cm^2 for the first order model system and (b) 13.8 MW/cm^2 for the second order model system.

system. Moreover, in the second order case, some adsorbates remain in the center of the coverage profile even at high laser intensities.

Changing the laser pulselength and maintaining a constant peak incident laser intensity significantly changes the coverage profiles as shown in fig. 6. The shorter pulselengths reach lower peak temperatures and maintain these peak temperatures for shorter durations. Consequently, the shorter pulselengths do not desorb as many adsorbates and create coverage profiles with smaller radii.

Another parameter that may be changed is the initial temperature of the surface. Fig. 7 shows the effect of changing the initial surface temperature. The initial surface temperature is important in determining the size of the resultant coverage profile because the laser-induced temperature rise adds to the initial

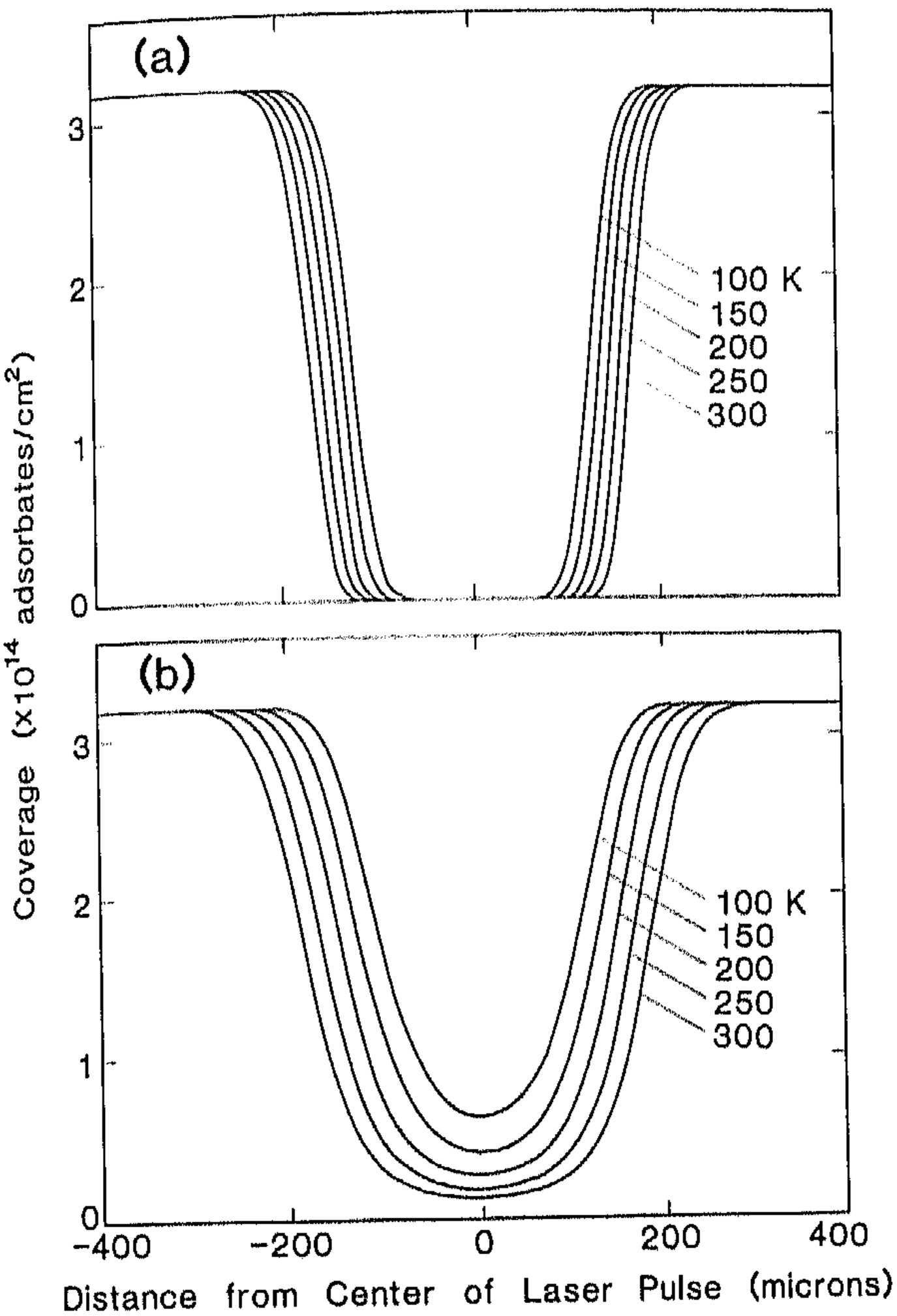

Fig. 7. The effect of the initial surface temperature on the resultant coverage profile. For (a) the first order model system and (b) the second order model system.

temperature. Higher initial temperatures lead to higher peak temperatures and the subsequent desorption of more adsorbates. The effect is the same for both the first and second order model systems.

3.4. *Effects of thermal desorption parameters*

The desorption activation energy and the pre-exponential for desorption will change for different adsorbate–substrate systems. Fig. 8 shows the effect of changing the desorption activation energy by increments of 5 kcal/mol with the pre-exponential fixed at 10^{13}/s and 10^{-3} cm^2/adsorbate · s. Very similar trends are observed when the pre-exponential is varied with the desorption

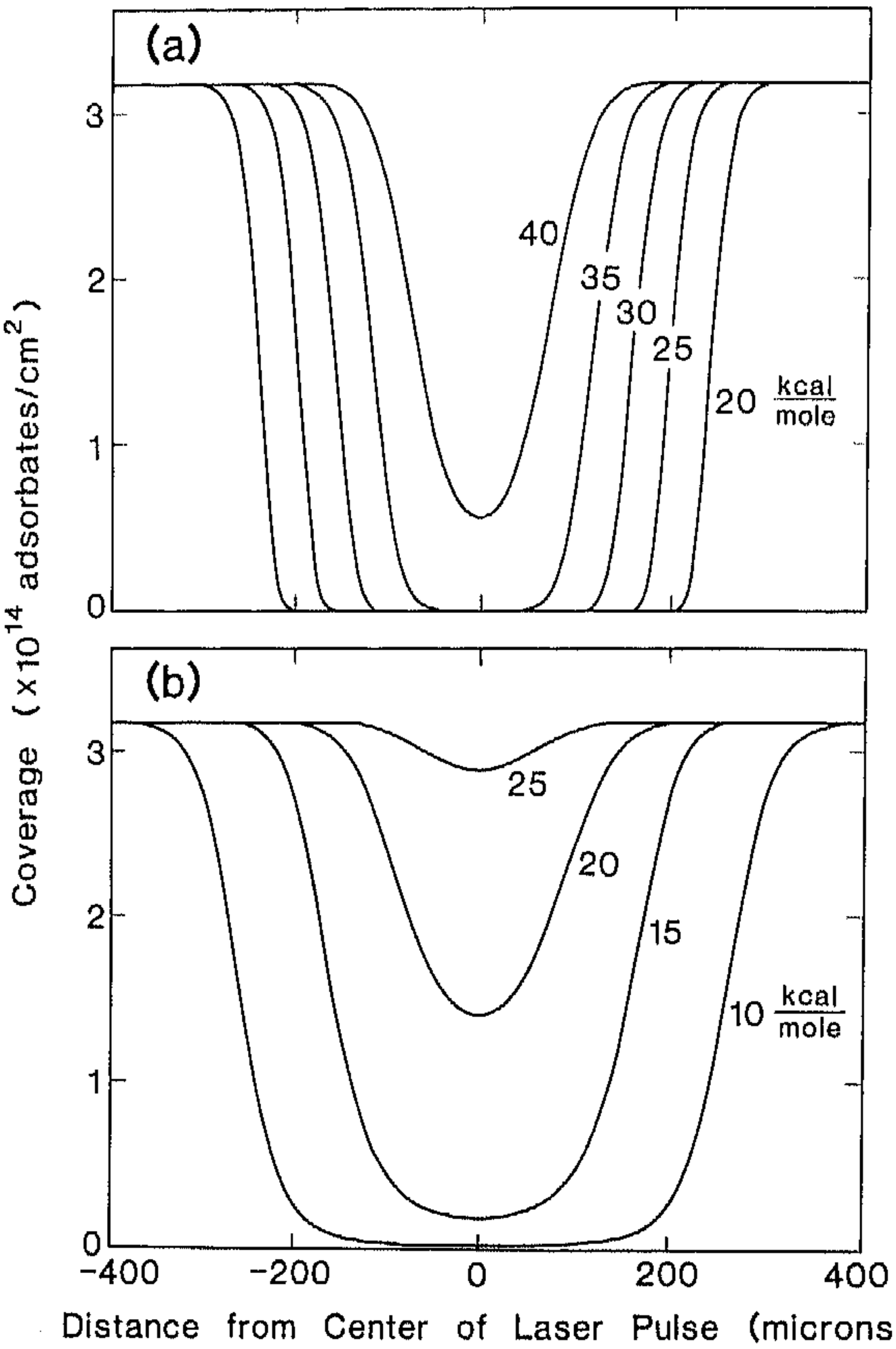

Fig. 8. The effect of the desorption activation energy on the resultant coverage profile for (a) the first order model system and (b) the second order model system.

activation energy fixed. Decreasing the desorption activation energy is similar in effect to increasing the pre-exponential.

4. Important relationships

4.1. Relationship between peak surface temperature and pulselength

In many LITD experiments, the peak temperature must be kept below the melting point of the surface. To prevent the surface from melting, the laser pulse energy may need to be reduced. This reduction will both decrease the size of the coverage profile and produce coverage profiles with more gently sloping edges, an undesirable characteristic for coverage gradient experiments. To

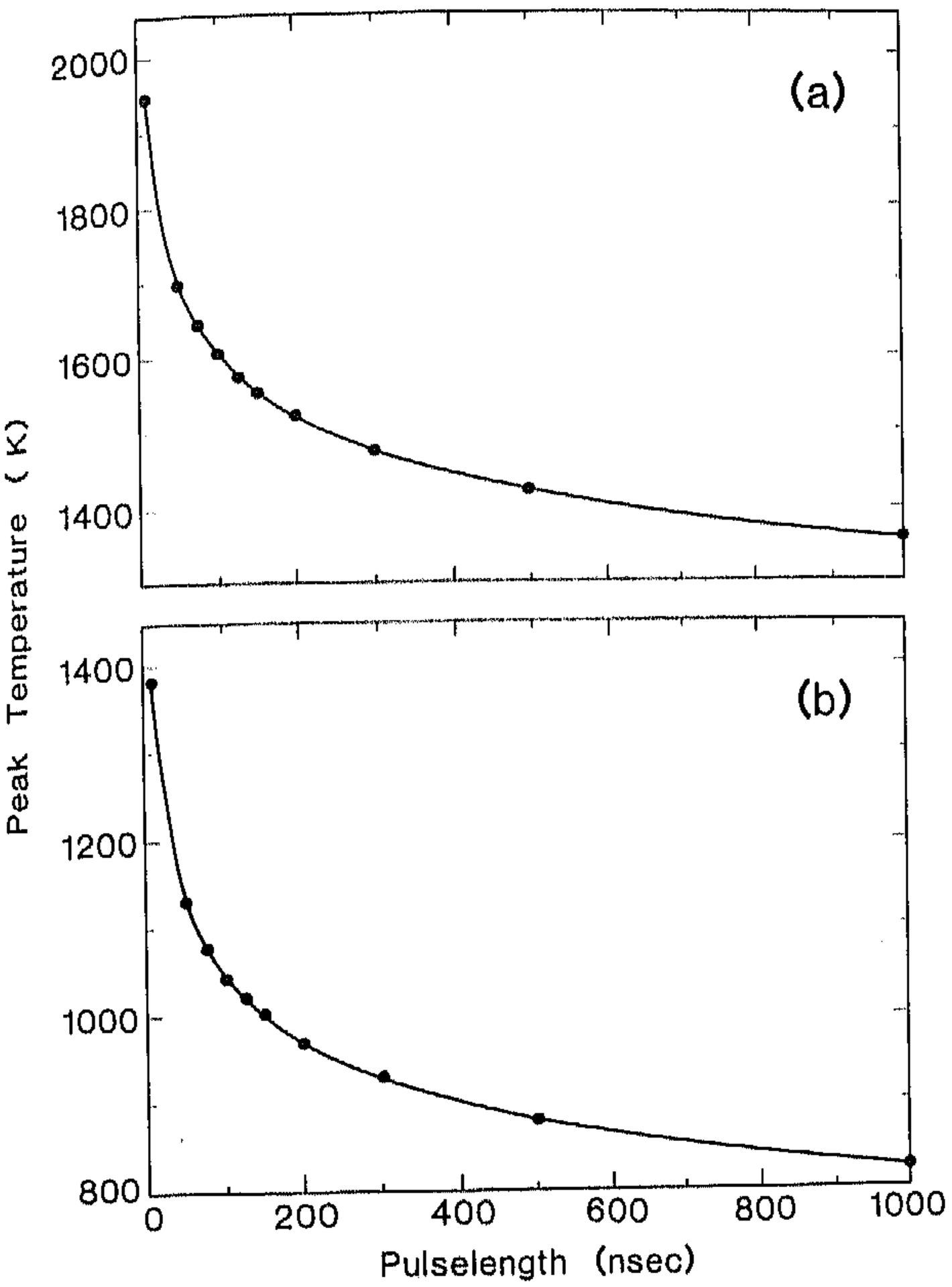

Fig. 9. The relationship between peak temperature and pulselength with the restriction that one-half the adsorbates are desorbed at $r = 0.4r_p$ for (a) the first order model system and (b) the second order model system.

avoid high temperatures and to maintain coverage profiles with larger radii, longer laser pulselengths can be used.

Using the criterion that one-half the adsorbates are desorbed at $r = 0.4r_p$, fig. 9 shows the relationship between the peak temperature and the pulselength. In order to avoid higher peak surface temperatures, there is a significant advantage to increasing the pulselength from 10 ns to 100 or 200 ns. Increasing the pulselength further to 1000 ns yields an additional, but smaller, decrease in the peak temperature.

Fig. 10b shows the spatial profiles of the peak temperatures that are reached for the different laser pulselengths in fig. 9. These various peak temperatures for different laser pulselengths are required in order to desorb one-half the adsorbates at $r = 0.4r_p$ and to obtain the coverage profile shown in fig. 10a. Parameters for the first order desorption model system were used in this calculation. Figs. 9 and 10 illustrate that there are advantages to using longer

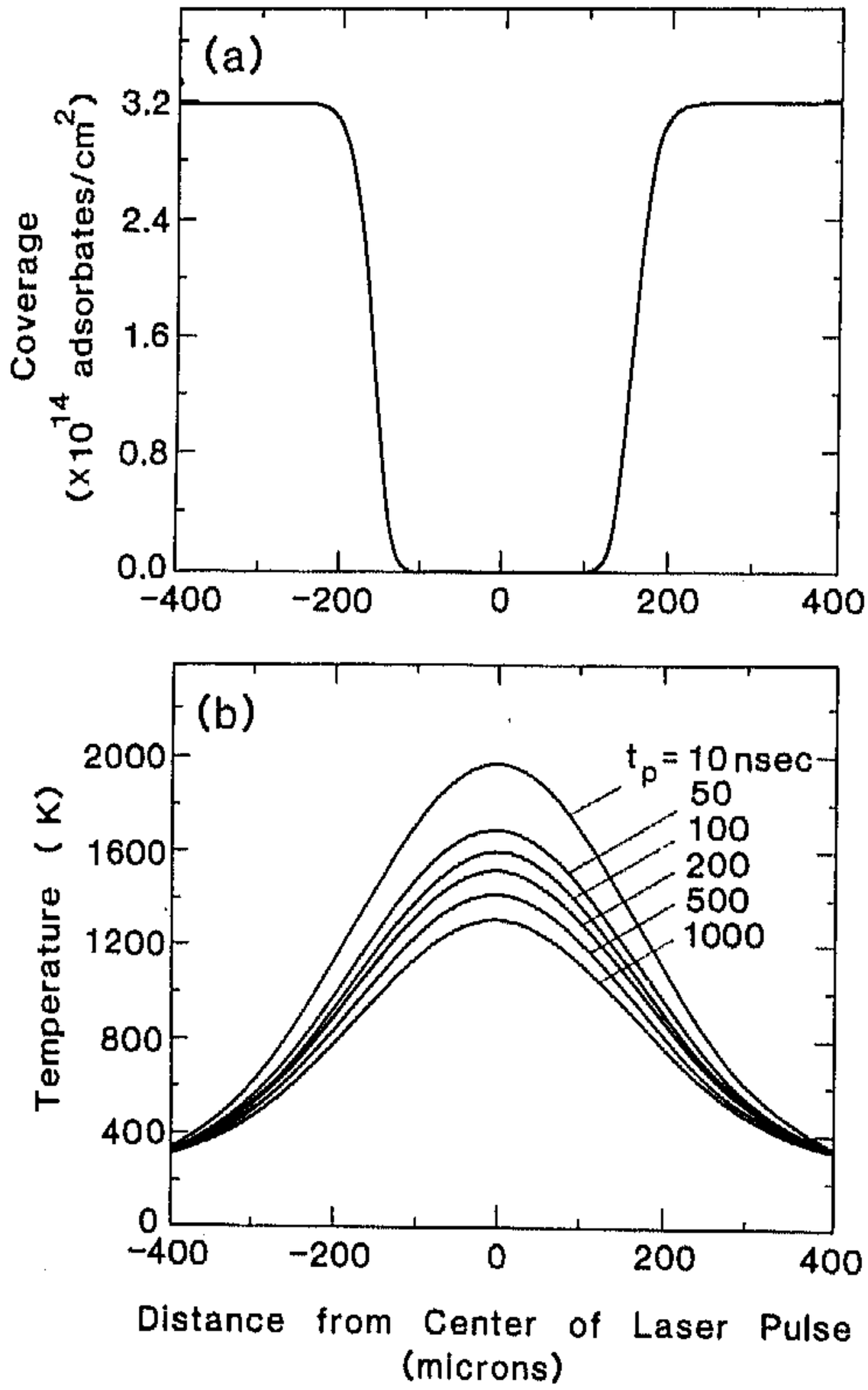

Fig. 10. The spatial profiles of the peak temperatures (shown in (b)) that were reached in order to desorb one-half the adsorbates at $r = 0.4r_p$ and to obtain the same coverage profile (shown in (a)) for the first order model system.

laser pulselengths. To obtain the same coverage profile, a shorter laser pulse must have a higher peak intensity and thus a higher peak temperature than for a longer pulselength. Consequently, longer pulselengths may be extremely important for surfaces with low melting points.

Nevertheless, for concentration gradient experiments, there are limits to increasing the pulselength. At pulselengths greater than $t_p = X^2/4\kappa$, where $X \simeq 0.1X_{exp}$ and X_{exp} is the experimental size of the desorption area, lateral heat diffusion becomes important. For these longer pulselengths, the laser heating can no longer be considered to be localized.

4.2. Relationship between desorption threshold and activation barrier

An intensity threshold must be reached before desorption may occur. Fig. 11 shows the relationship between the peak laser intensity and the desorption

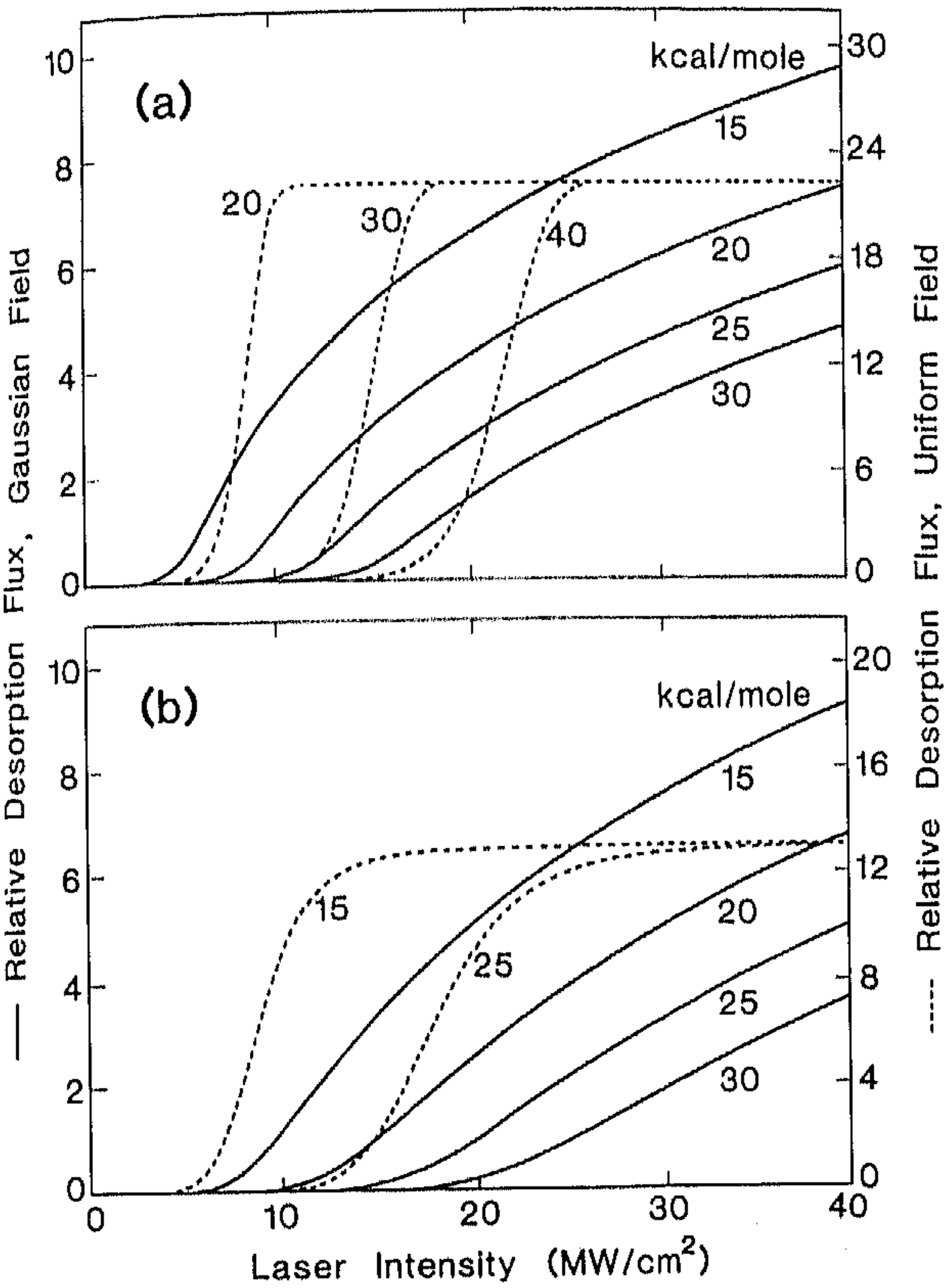

Fig. 11. The total number of adsorbates desorbed versus the peak incident laser intensity for (a) the first order model system and (b) the second order model system.

flux for various desorption activation barriers. Similar calculated results have been reported [15,28]. In the few cases where measurements have been made, the results display the same functional form as these calculations [15,20,28]. Measuring the intensity threshold provides a method to determine the desorption activation energy if a pre-exponential is assumed.

A uniform spatial distribution displays a very different dependence of the desorption flux on the peak laser intensity as shown in fig. 11. For a uniform spatial distribution confined to a definite area, the resulting coverage profile is a simple step function at the edge of the uniform field. Consequently, at higher laser intensities, the desorption yield is limited to the number of adsorbates in the irradiated area. As a probe of the desorption activation energy, a uniform spatial distribution is more sensitive than a Gaussian spatial distribution. Furthermore, a measurement of the desorption yield as a function of laser intensity provides a means to verify the spatial distribution.

4.3. Relationship between peak temperature and activation barrier

The melting point of a surface generally establishes an upper bound on the maximum peak temperature. Consequently, knowing the peak temperature that must be reached in order to desorb an adsorbate with a given activation energy for desorption is important. Fig. 12 shows the relationship between peak temperature and desorption activation barrier for the two model systems as a function of pulselength. Each point on this graph gave rise to the same size coverage profile. The size of the coverage profile is such that one-half of the initial adsorbates were desorbed at $r = 0.4r_p$. Changing the initial surface temperature to 0 K from 250 K required an increase in the peak temperature of only 50 to 100 K to create the same size coverage profile.

Similar graphs for a uniform spatial distribution of the laser can be generated. In this case a different criterion to define the extent of desorption

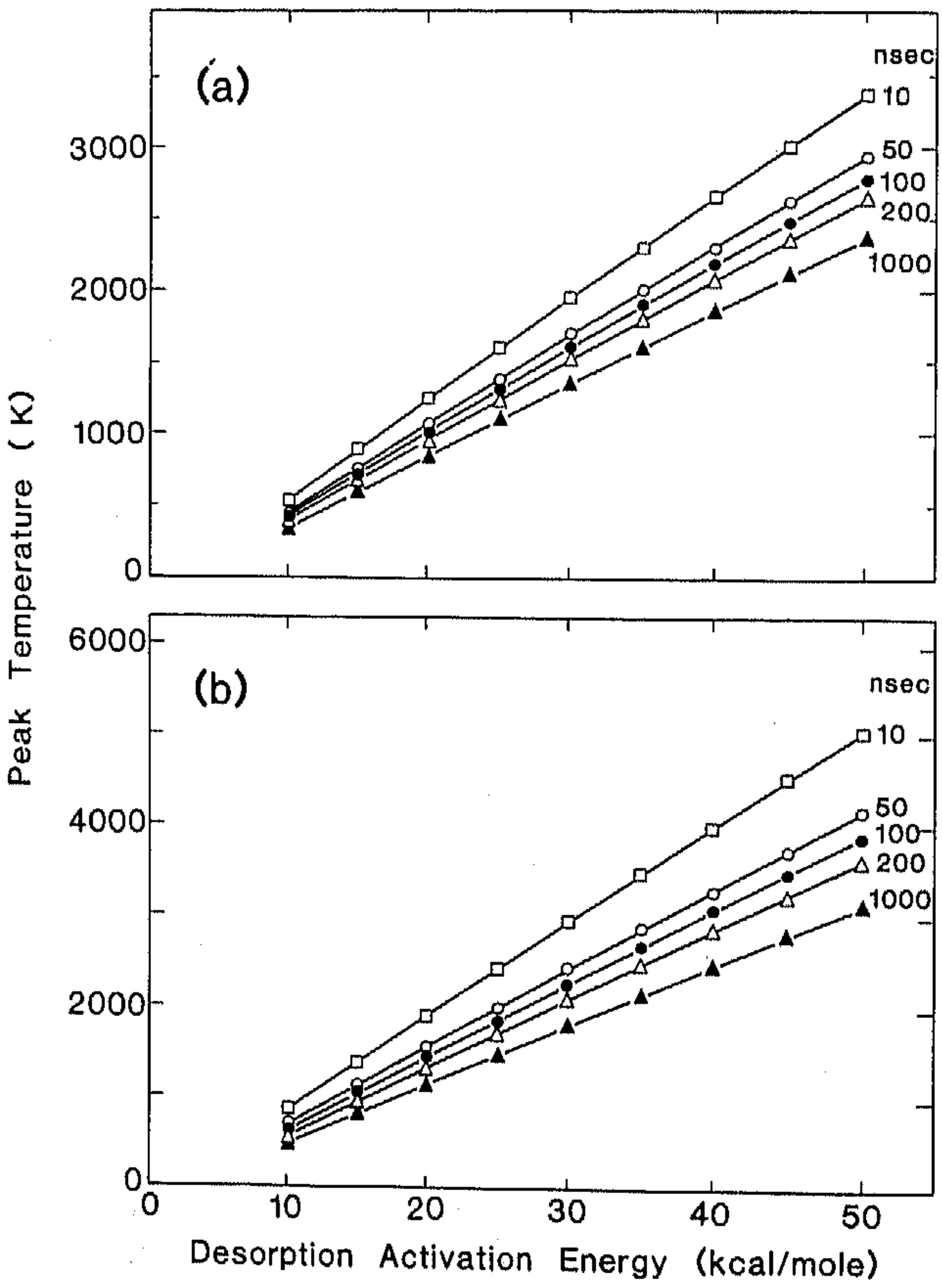

Fig. 12. The relationship between the peak temperature and the desorption activation energy for various pulselengths for (a) the first order model system and (b) the second order model system.